Inertial Sensor Bias Estimation in GPS/INS Integration through Nonlinear Kalman Filtering

Article · June 2012

CITATIONS
0

READS
3,033

3 authors:

Yong Li
UNSW Sydney
48 PUBLICATIONS **709** CITATIONS
SEE PROFILE

Jinling Wang
UNSW Sydney
382 PUBLICATIONS **8,381** CITATIONS
SEE PROFILE

Chris Rizos
UNSW Sydney
697 PUBLICATIONS **13,163** CITATIONS
SEE PROFILE

Inertial Sensor Bias Estimation in GPS/INS Integration through Nonlinear Kalman Filtering

Yong Li, Jinling Wang, and Chris Rizos
(University of New South Wales, Sydney 2052, Australia)
Email: yong.li@unsw.edu.au

The GPS/INS integration system estimates the navigation errors as well as internal sensor errors through the use of a Kalman filter. The tight integration processing mode uses the GPS range and range-rate measurements in a nonlinear Kalman filter. Extended Kalman filtering (EKF) has been discussed in many publications dealing with GPS/INS integration. The recently developed sigma-point Kalman filtering algorithm has advantages over the EKF, for instance by its ability to capture the high-order nonlinear terms without requiring the computation of the Jacobian matrix.

INS sensor calibration usually occurs during the INS initialisation process. Integration of GPS and INS adds potential in-flight alignment capability to the system. This paper concentrates on the inertial sensor error estimation via nonlinear Kalman filtering, using both the EKF and the SPKF. A procedure for the inertial sensor bias estimation is proposed that is based on an observability analysis of the tight integration system. In addition, an algorithm for the coarse estimation of the inertial sensor biases is proposed. The performances of the SPKF and the EKF for the fine alignment are compared.

KEY WORDS:
1. GPS/INS integration, 2. Extended Kalman filter, 3. Sigma-point Kalman filter, 4. Sensor bias estimation

1. INTRODUCTION

As is well known, the integration of GPS and INS can overcome the shortcomings of INS or GPS standalone systems. Depending on the type of GPS data used in the integration, the system integration can be categorised according to different levels, e.g. tight integration uses the GPS range and range-rate measurements, while loose integration uses the GPS position and/or velocity solution. The so-called ultra-tight integration or deep integration approach uses the integration solution to aid the GPS signal acquisition and the receiver tracking loops. The main advantage of tight integration over the loose integration approach is that it can continuously correct the INS errors even if the number of visible GPS satellites drops below four.

In tight integration designs different GPS measurements can be used to achieve different accuracy levels. Utilisation of the carrier phase measurements can achieve a solution of the highest accuracy [1]. The pseudorange and Doppler measurements can be used in applications suitable for low-cost, medium-precision integration systems [2-4].

Tight integration design introduces nonlinear terms into the integration Kalman filter, e.g. the nonlinear issues arise from the range and range-rate observation equations. Most state-of-the-art GPS/INS integration systems are designed to calibrate the INS errors, based on the INS error state propagation in the Kalman filter. This scheme has been demonstrated by many successful systems and their applications over the past two decades [2][3]. Recently the application of nonlinear filtering methods to integrated navigation has been investigated [4][5]. In these investigations either the differential equation of the INS mechanisation or the kinematical equations of the host platform is chosen as the system dynamics model. This design unavoidably introduces nonlinearities into the filtering system, even for a loosely-coupled GPS/INS integration system.

The extended Kalman filter is the “standard” approach for state estimation of nonlinear systems during the past few decades [6]. The basis of the EKF is linearisation of the system equation and/or the observation equation around either the previous estimate or the current prediction. The linearised system is then represented by the Jacobians of the nonlinear system/measurement functions. The standard Kalman filtering formulae are applied to the linearised system. However, the procedure produces sub-optimal estimates of the system states. The EKF has some defects, such as it is challenging to

implement, difficult to tune, and the first-order term may be insufficiently accurate to approximate the nonlinearities of the system [7].

The sigma-point Kalman filter was developed to overcome the limitations of the EKF. Distinguishing itself from the standard Kalman filter, the SPKF calculates the filtering parameters using a set of sampling-like points - the so-called “sigma points” - which can be mapped into the state space or the measurement space through the nonlinear functions of the system directly, instead of linearisation through the Jacobians. The parameters derived from the sigma points include the SPKF gain matrix, the state prediction and its covariance, the measurement prediction and its covariance, as well as the estimate covariance [7-9].

Discussions concerning the performance of the EKF and the SPKF-based tight integration for navigation solution estimation can be found in [4] [10]. The filtering solution, including the INS solution errors as well as the sensor biases, are often fed back into the strapdown INS (SDINS) calculation. A small error in the sensor bias estimates could cause a large error in the navigation solution. Thus the feedback correction has a rigorous requirement as far as the accuracy of the filter’s estimates is concerned. This paper investigates the performance of the EKF and the impact of the SPKF on the inertial sensor bias estimation. A procedure for inertial sensor bias estimation is proposed that is based on the analysis of the system observability of tight integration. An algorithm for the coarse estimation of the inertial sensor biases is proposed as well.

The paper is organised as follows. First it summarises the mathematical bases of the two nonlinear filters, the EKF and the SPKF. Then a method is presented for the coarse estimation of the inertial sensor biases from the measurements of the accelerometers and gyros. The ability of the integration filter to estimate the sensor bias is analysed using the control theory approach. A procedure for sensor bias estimation is proposed. The tests results are then presented.

2. OPTIMAL ESTIMATION FOR NONLINEAR SYSTEMS

Consider the nonlinear discrete-time system

$$\mathbf{x}(k+1) = \mathbf{f}[\mathbf{x}(k), k] + \mathbf{G}(k+1, k)\mathbf{w}(k) \tag{1}$$

$$\mathbf{z}(k+1) = \mathbf{h}[\mathbf{x}(k+1), k+1] + \mathbf{v}(k+1) \tag{2}$$

where $\mathbf{x}(k)$ is the state of the system at k, and $\mathbf{z}(k)$ is the measurement vector. The vectors $\mathbf{w}(k)$ and $\mathbf{v}(k)$ are the system noise and measurement noise respectively.

2.1 Extended Kalman Filter.

The EKF applies the Kalman filter to nonlinear systems by simply linearising all the nonlinear models so that the traditional linear Kalman filter equations can be applied. The extended Kalman filter (EKF) gives the estimate and the covariance [6]

$$\hat{\mathbf{x}}(k+1|k+1) = \hat{\mathbf{x}}(k+1|k) + \mathbf{K}(k+1)[\mathbf{z}(k+1) - \hat{\mathbf{z}}(k+1|k)] \tag{3}$$

$$\mathbf{P}(k+1|k+1) = [\mathbf{I} - \mathbf{K}(k+1)\mathbf{H}(k+1)]\mathbf{P}(k+1|k) \tag{4}$$

The prediction of the states and its covariance are

$$\hat{\mathbf{x}}(k+1|k) = \mathbf{f}[\hat{\mathbf{x}}(k|k), k] \tag{5}$$

$$\mathbf{P}(k+1|k) = \mathbf{F}(k+1, k)\mathbf{P}(k|k)\mathbf{F}^{\mathrm{T}}(k+1, k) + \mathbf{G}(k+1, k)\mathbf{Q}(k)\mathbf{G}^{\mathrm{T}}(k+1, k) \tag{6}$$

The prediction of measurements is

$$\hat{\mathbf{z}}(k+1|k) = \mathbf{h}[\hat{\mathbf{x}}(k+1|k), k+1] \tag{7}$$

The Kalman gain matrix is

$$\mathbf{K}(k+1) = \mathbf{P}(k+1|k)\mathbf{H}^{\mathrm{T}}(k+1)[\mathbf{H}(k+1)\mathbf{P}(k+1|k)\mathbf{H}^{\mathrm{T}}(k+1) + \mathbf{R}(k+1)]^{-1} \tag{8}$$

where **F**(k+1,k) and **H**(k+1) are the Jacobian matrices associated with **f** and **h,** respectively

$$\mathbf{F}(\mathrm{k}+1,\mathrm{k}) = \frac{\partial}{\partial \mathbf{x}}\mathbf{f}[\hat{\mathbf{x}}(\mathrm{k}|\mathrm{k}),\mathrm{k}] \tag{9}$$

$$\mathbf{H}(\mathrm{k}+1) = \frac{\partial}{\partial \mathbf{x}}\mathbf{h}[\hat{\mathbf{x}}(\mathrm{k}+1|\mathrm{k}),\mathrm{k}+1] \tag{10}$$

2.2 Sigma-point Kalman Filter

The sigma-point Kalman filter, according to [7-9], can be summarised as follows. The SPKF updates the predication after the measurements are made:

$$\hat{\mathbf{x}}(\mathrm{k}+1|\mathrm{k}+1) = \hat{\mathbf{x}}(\mathrm{k}+1|\mathrm{k}) + \mathbf{S}(\mathrm{k}+1)[\mathbf{z}(\mathrm{k}+1) - \hat{\mathbf{z}}(\mathrm{k}+1|\mathrm{k})] \tag{11}$$

Comparing Eq. (11) with Eq. (3), one can see that the SPKF has the same prediction-correction structure as the standard Kalman filter. The gain matrix **S** in Eq. (11) can be referred to as the SPKF gain matrix, in a similar way to the Kalman filter's gain matrix **K** in Eq. (3). The covariance of the estimates is

$$\mathbf{P}(\mathrm{k}+1|\mathrm{k}+1) = \mathbf{P}(\mathrm{k}+1|\mathrm{k}) - \mathbf{S}(\mathrm{k}+1)\cdot[\mathbf{R}(\mathrm{k}+1) + \mathbf{P}_{zz}(\mathrm{k}+1|\mathrm{k}+1)]\mathbf{S}^{\mathrm{T}}(\mathrm{k}+1) \tag{12}$$

The SPKF gain matrix **S** is

$$\mathbf{S}(\mathrm{k}+1) = \mathbf{P}_{\mathrm{xz}}(\mathrm{k}+1|\mathrm{k})[\mathbf{R}(\mathrm{k}+1) + \mathbf{P}_{zz}(\mathrm{k}+1|\mathrm{k}+1)]^{-1} \tag{13}$$

For a system described by an n-dimensional state, 2n+1 sigma points will be used. Details of the reduced SPKF can be found in [11]. Hereafter the normal 2n+1 sigma points will be used. The sigma points in the state space and associated weights are

$$\mathbf{X}_0(\mathrm{k}|\mathrm{k}) = \hat{\mathbf{x}}(\mathrm{k}|\mathrm{k}), \quad \mathrm{W}_0 = \kappa/\{\mathrm{n}+\kappa\} \tag{14}$$

$$\mathbf{X}_{\mathrm{i}}(\mathrm{k}|\mathrm{k}) = \hat{\mathbf{x}}(\mathrm{k}|\mathrm{k}) + \sqrt{(\mathrm{n}+\kappa)\mathbf{P}(\mathrm{k}|\mathrm{k})}\,, \mathrm{W}_{\mathrm{i}} = 0.5/(\mathrm{n}+\kappa) \tag{15}$$

$$\mathbf{X}_{\mathrm{i+n}}(\mathrm{k}|\mathrm{k}) = \hat{\mathbf{x}}(\mathrm{k}|\mathrm{k}) - \sqrt{(\mathrm{n}+\kappa)\mathbf{P}(\mathrm{k}|\mathrm{k})}\,, \mathrm{W}_{\mathrm{i+n}} = 0.5/(\mathrm{n}+\kappa) \tag{16}$$

The sigma points of predication are then

$$\mathbf{X}_{\mathrm{i}}(\mathrm{k}+1|\mathrm{k}) = \mathbf{f}[\mathbf{X}_{\mathrm{i}}(\mathrm{k}|\mathrm{k}),\mathrm{k}] \tag{17}$$

The predication and its covariance are

$$\hat{\mathbf{x}}(\mathrm{k}+1|\mathrm{k}) = \sum_{\mathrm{i}=0}^{2\mathrm{n}} \mathrm{W}_{\mathrm{i}}\mathbf{X}_{\mathrm{i}}(\mathrm{k}+1|\mathrm{k}) \tag{18}$$

$$\mathbf{P}(\mathrm{k}+1|\mathrm{k}) = \sum_{\mathrm{i}=0}^{2\mathrm{n}} \mathrm{W}_{\mathrm{i}}[\mathbf{X}_{\mathrm{i}}(\mathrm{k}+1|\mathrm{k}) - \hat{\mathbf{x}}(\mathrm{k}+1|\mathrm{k})][\mathbf{X}_{\mathrm{i}}(\mathrm{k}+1|\mathrm{k}) - \hat{\mathbf{x}}(\mathrm{k}+1|\mathrm{k})]^{\mathrm{T}} \tag{19}$$

The sigma points of measurements are

$$\mathbf{Z}_{\mathrm{i}}(\mathrm{k}+1|\mathrm{k}) = \mathbf{h}[\mathbf{X}_{\mathrm{i}}(\mathrm{k}+1|\mathrm{k}),\mathrm{k}+1] \tag{20}$$

The prediction of measurements and their covariance are

$$\hat{\mathbf{z}}(\mathrm{k}+1|\mathrm{k}) = \sum_{\mathrm{i}=0}^{2\mathrm{n}} \mathrm{W}_{\mathrm{i}}\mathbf{Z}_{\mathrm{i}}(\mathrm{k}+1|\mathrm{k}) \tag{21}$$

$$\mathbf{P}_{zz}(k+1|k) = \sum_{i=0}^{2n} W_i[\mathbf{Z}_i(k+1|k) - \hat{\mathbf{z}}(k+1|k)][\mathbf{Z}_i(k+1|k) - \hat{\mathbf{z}}(k+1|k)]^T \tag{22}$$

$$\mathbf{P}_{xz}(k+1|k) = \sum_{i=0}^{2n} W_i[\mathbf{X}_i(k+1|k) - \hat{\mathbf{x}}(k+1|k)][\mathbf{Z}_i(k+1|k) - \hat{\mathbf{z}}(k+1|k)]^T \tag{23}$$

3. COARSE ESTIMATION OF SENSOR BIASES

3.1 Gyro Bias Estimation

The gyros sense the rotation rate of the host platform (b-frame) with respect to the inertial system (i-frame). The measurement equation of the gyros can be written as

$$\hat{\omega}_{ib} = \omega_{ib} + \boldsymbol{\varepsilon} + \xi \tag{24}$$

where $\boldsymbol{\varepsilon}$ is the gyro bias, ξ is the measurement noise, and ω_{ib} is the true angular velocity of the b-frame with respect to the i-frame

$$\omega_{ib} = \omega_{ie} + \omega_{en} + \omega_{nb} \tag{25}$$

Substituting Eq. (25) into Eq. (24) and expressing the vectors in the b-frame or the n-frame correspondingly yields

$$\hat{\omega}_{ib}^b = \mathbf{C}_n^b\left(\omega_{ie}^n + \omega_{en}^n\right) + \omega_{nb}^b + \boldsymbol{\varepsilon}^b + \xi \tag{26}$$

where $\mathbf{C}_n^b$ is the direction cosine matrix (DCM) which transforms a vector from the n-frame to the b-frame.

When the inertial measurement unit (IMU) is at rest, the angular velocities $\omega_{en}^n = 0$ and $\omega_{nb}^b = 0$. Eq. (26) can be simplified as

$$\hat{\omega}_{ib}^b = \mathbf{C}_n^b\omega_{ie}^n + \boldsymbol{\varepsilon}^b + \xi \tag{27}$$

If the b-frame is almost aligned with the n-frame, the DCM can be expressed as [12]

$$\mathbf{C}_n^b = \mathbf{I} + \phi\times \tag{28}$$

where ϕ is the misalignment angular vector.

Substituting Eq. (28) into Eq. (27) yields

$$\hat{\omega}_{ib}^b = \omega_{ie}^n + \phi\times\omega_{ie}^n + \boldsymbol{\varepsilon}^b + \xi \tag{29}$$

After alignment, the misalignment is a small value. The second term on the right-hand side of Eq. (29) can be treated as a higher order term and ignored. The gyro bias measurement equation is then

$$\hat{\boldsymbol{\varepsilon}}^b = \hat{\omega}_{ib}^b - \omega_{ie}^n - \xi \tag{29}$$

where the earth rotation rate expressed in the n-frame is

$$\omega_{ie}^n = \begin{bmatrix} \Omega_e \cos L \\ 0 \\ -\Omega_e \sin L \end{bmatrix} \tag{30}$$

where L is the local latitude.

Eq. (29) can be used to estimate the gyro biases. The estimation error is obtained by comparing Eqs. (29) and (30)

$$\delta\boldsymbol{\varepsilon}^b = \hat{\boldsymbol{\varepsilon}}^b - \boldsymbol{\varepsilon}^b = \phi \times \omega_{ie}^n = \Omega_e \begin{bmatrix} \phi_x \sin L \\ \phi_x \sin L + \phi_z \cos L \\ -\phi_y \cos L \end{bmatrix} \tag{31}$$

It is clear that the tilt errors impact on north and vertical components, while the azimuth error impacts on the east component only. The tilt angles can be obtained using the accelerometers' output. The azimuth can be obtained using high quality gyro measurements through gyro-compassing, or using magnetometer measurements [13].

3.2 Accelerometer Bias Estimation

The accelerometers sense the specific force of the host platform. The measurement equation of the accelerometers can be written as

$$\hat{\mathbf{f}}^b = \mathbf{f}^b + \nabla^b + \zeta \tag{32}$$

where ∇ is the accelerometer bias, ζ is the measurement noise, and $\mathbf{f}$ is the true specific force.

According to the INS velocity equation [14]

$$\mathbf{f}^n = \dot{\mathbf{v}}^n + \left(2\boldsymbol{\omega}_{ie}^n + \boldsymbol{\omega}_{en}^n\right) \times \mathbf{v}^n - \mathbf{g}^n \tag{33}$$

substituting Eq. (33) into Eq. (32) yields

$$\hat{\mathbf{f}}^b = \mathbf{C}_n^b \left(\dot{\mathbf{v}}^n + \left(2\boldsymbol{\omega}_{ie}^n + \boldsymbol{\omega}_{en}^n\right) \times \mathbf{v}^n - \mathbf{g}^n\right) + \nabla^b + \zeta \tag{34}$$

When the INS is at rest, Eq. (34) can be further simplified as

$$\hat{\mathbf{f}}^b = -\mathbf{C}_n^b \mathbf{g}^n + \nabla^b + \zeta \tag{35}$$

Substituting Eq. (28) into Eq. (35) yields

$$\hat{\mathbf{f}}^b = -\mathbf{g}^n - \phi \times \mathbf{g}^n + \nabla^b + \zeta \tag{36}$$

Given the fact that the misalignment is a small value after INS alignment, the second term on the right-hand side of Eq. (30) can be ignored (assumed to be a higher order term). The accelerometer bias measurement equation is then written as

$$\hat{\nabla}^b = \hat{\mathbf{f}}^b + \mathbf{g}^n - \zeta \tag{37}$$

where

$$\mathbf{g}^n = \begin{bmatrix} 0 & 0 & g \end{bmatrix}^T \tag{38}$$

Eq. (37) can be used to estimate the accelerometer biases. The estimation error is obtained by comparing Eqs. (36) and (37)

$$\delta\nabla^b = \hat{\nabla}^b - \nabla^b = -\phi \times \mathbf{g}^n = g\begin{bmatrix} -\phi_y \\ \phi_x \\ 0 \end{bmatrix} \tag{39}$$

It is clear that the tilt errors impact on the north and east components, while the azimuth error does not introduce any errors into the estimates. The misalignment does not impact on the vertical component.

4. ESTIMATION OF SENSOR BIASES BY THE INTEGRATION KALMAN FILTER

A tightly-coupled GPS/INS integration is a nonlinear system, and the observation equation may have different forms for different filtering methods. The EKF linearises the system around the prediction of the state vector. The SPKF does not need to linearise the system, and the nonlinear functions of the system are directly used in the algorithm for generating the sigma points. The 15 states of the filter include the INS error states and the sensor error states.

The INS psi-angle error model is used as the state equation [15]

$$\delta\dot{\mathbf{r}} = -\omega_{en} \times \delta\mathbf{r} + \delta\mathbf{v} \tag{40}$$
$$\delta\dot{\mathbf{v}} = -(\omega_{ie} + \omega_{in}) \times \delta\mathbf{v} + \mathbf{f} \times \psi + \nabla + \Delta\mathbf{g} \tag{41}$$
$$\dot{\psi} = -\omega_{in} \times \psi + \boldsymbol{\varepsilon} \tag{42}$$

The sensor errors are modelled as random walk processes

$$\dot{\nabla} = w_{\nabla} \tag{43}$$
$$\dot{\boldsymbol{\varepsilon}} = w_{\varepsilon} \tag{44}$$

where $\delta\mathbf{r}$, $\delta\mathbf{v}$, and ψ are the error vectors of position, velocity and angle, respectively. ∇ and ε are the errors of the accelerometers and gyros, respectively.

The system equation of the integration Kalman filter can be written as

$$\dot{\mathbf{x}} = \mathbf{F}\mathbf{x} + \mathbf{B}\mathbf{u} + \mathbf{G}\mathbf{w} \tag{45}$$

where the state vector is

$$\mathbf{x} = \begin{bmatrix} \delta\mathbf{r} & \delta\mathbf{v} & \psi & \nabla & \boldsymbol{\varepsilon} \end{bmatrix}^T \tag{46}$$

The matrix **F** is

$$\mathbf{F} = \begin{bmatrix} \mathbf{F}_{pp} & \mathbf{F}_{pv} & \mathbf{0} & \mathbf{0} & \mathbf{0} \\ \mathbf{F}_{vp} & \mathbf{F}_{vv} & \mathbf{F}_{v\psi} & \mathbf{C}_b^n & \mathbf{0} \\ \mathbf{0} & \mathbf{0} & \mathbf{F}_{\psi\psi} & \mathbf{0} & \mathbf{C}_b^n \\ \mathbf{0} & \mathbf{0} & \mathbf{0} & \mathbf{0} & \mathbf{0} \\ \mathbf{0} & \mathbf{0} & \mathbf{0} & \mathbf{0} & \mathbf{0} \end{bmatrix} \tag{47}$$

The sub-block matrices can be derived from the psi-angle model using Eqs. (40) to (42).

The observation equations for the EKF and the SPKF can be found in [10]. For example, for the EKF, the measurement equations can be written as

$$\mathbf{z} = \mathbf{H}\mathbf{x} + \eta \tag{48}$$

where **z** is the measurement vector consisting of the range and range-rate measurements from all visible satellites, η is the measurement noise, and **H** is the Jacobian matrix

$$\mathbf{H} = \begin{bmatrix} \cdots & \mathbf{H}_i^T & \cdots \end{bmatrix}^T \tag{49}$$

The block matrix $\mathbf{H}_i$ is a 2 by n matrix associated with the i^{th} visible satellite

$$\mathbf{H}_i = \begin{bmatrix} \dfrac{\left(\mathbf{r}_{sat}^i - \mathbf{r}_{ins} + \delta\hat{\mathbf{r}}_{k|k-1}\right)^T}{\left\|\mathbf{r}_{sat}^i - \mathbf{r}_{ins} + \delta\hat{\mathbf{r}}_{k|k-1}\right\|} & \mathbf{0} & \mathbf{0} \\ \dfrac{\left(\mathbf{v}_{sat}^i - \mathbf{v}_{ins} + \delta\hat{\mathbf{v}}_{k|k-1}\right)^T}{\left\|\mathbf{r}_{sat}^i - \mathbf{r}_{ins} + \delta\hat{\mathbf{r}}_{k|k-1}\right\|} & \dfrac{\left(\mathbf{r}_{sat}^i - \mathbf{r}_{ins} + \delta\hat{\mathbf{r}}_{k|k-1}\right)^T}{\left\|\mathbf{r}_{sat}^i - \mathbf{r}_{ins} + \delta\hat{\mathbf{r}}_{k|k-1}\right\|} & \mathbf{0} \end{bmatrix} \tag{50}$$

Using range and range-rate measurements, the position error and velocity error are directly observable. Thus the observability analysis of the system is of most interest. Only when the system is completely observable can the rest states such as the angular error and sensor biases be estimated from the range and range-rate measurements. The system (**F**, **H**) described by Eqs. (45) and (48) is observable if the observability matrix below is non-singular [16]

$$\Theta = \begin{bmatrix} \mathbf{H} \\ \mathbf{HF} \\ \vdots \\ \mathbf{HF}^{n-1} \end{bmatrix} \tag{51}$$

The system is completely observable if the rank of the observability matrix is equal to the system dimension, i.e.

$$\text{rank}(\Theta) = \text{n} \tag{52}$$

This means that the angular error as well as the sensor biases are all observable within the Kalman filter. However, if the rank of the observability matrix is less than n, this means that some of the state components are unobservable within the Kalman filter. As a result the standard deviation of all state estimates that are not directly measured can not decrease below a certain bound [15]. For GPS/INS integration, the states may be non-orthogonal to each other, the angular error and the sensor biases are therefore partially observable even if the system is not completely observable.

Theoretically deriving the analytical solution of Eq. (51) is very difficult. A numerical approach is used in this paper. The rank of the observability matrix is calculated at each filtering step. Fig. 1 illustrates the result.

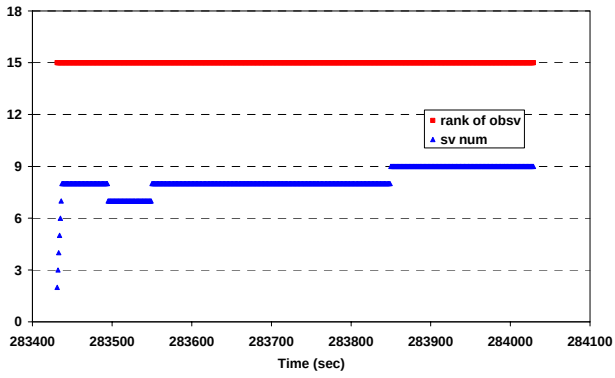

Fig. 1 The rank of the observability matrix vs. time

The rank of the observability matrix is equal to 15, the dimension of the system state vector, at all epochs, even when the number of visible satellites is less than 4. This means that the tightly-integrated system is completely observable, or in other words the sensor biases can be re-constructed or estimated from the range and range-rate measurements.

The data processing can be divided into three steps: (1) the coarse alignment; (2) the fine alignment; and (3) the strapdown INS and integration Kalman filtering. During coarse alignment, the tilt angles are computed from the accelerometer data, and the azimuth angle can be computed from gyro-compassing or by other methods. A coarse estimate of the sensor biases is obtained during the alignment. The Kalman filter further estimates the error estimates and attempts to derive a better estimate. The flowchart of the procedure is shown in Fig. 2.

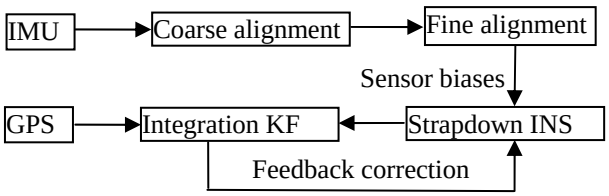

Fig. 2 Flowchart of the procedure

5. TESTS

A field programmable gate array (FPGA) based GPS/INS data logging device was used for collecting and time-synchronising the GPS and INS data. The device has been developed under the Australian Cooperative Research Centre (CRC) for Spatial Information (CRC-SI) project 1.3 “Integrated Positioning and Geo-referencing Platform”. The objective of this project is to develop a generic hardware and software platform for positioning and imaging sensor integration. The GPS and INS data was recorded onto a compact flash card. The data was then further processed by the software to estimate the INS errors via the integration Kalman filter. Details of the project can be found in [17].

The tests presented here focus on the capability of the integration Kalman filter for sensor bias estimation. The hardware setup in the laboratory is depicted in Fig. 3. Boeing's C-MIGITS II is used as a standalone INS device to provide inertial data. An Allstar GPS receiver was selected for the tight integration because of its stable PPS output and easy-to-use message format. The C-MIGITS II was configured to output 10Hz raw IMU data ($\Delta\mathbf{v}$ and $\Delta\boldsymbol{\theta}$) in the tests. The Allstar was configured to output the raw measurements, including the pseudorange and Doppler, and the satellite broadcast ephemeris.

Fig. 3 Device setup in the laboratory

The results of coarse estimation of the sensor biases from a series of tests are listed in Tables 1 and 2 - the 3D accelerometer biases in Table 1, and the 3D gyro biases in Table 2. During the tests the C-MIGITS II was mounted horizontally on a table with an approximate heading to the North. The coarse alignment process runs for 100 seconds. An infinite impulse response (IIR) low-pass filter was used to smooth the estimates. The estimates were fixed to the value obtained at the end of the

alignment process. The time history of estimates of the accelerometers and gyros are shown in Figs. 4 and 5. Note that the results in Tables 1 and 2 and Figs 4 and 5 are the biases at 0.1s intervals. Thus the unit for accelerometer bias is m/s, and the gyro bias has a unit of radians.

Table 1 Coarse estimation of 3D accelerometer biases

Test	Accl biases in BF (m/s)		
	x	y	z
060531	-9.76e-3	9.32e-3	-9.0e-4
060601	-9.54e-3	9.21e-3	-1.45e-3
060607	-7.18e-3	1.07e-2	-1.39e-3
060608	-1.68e-2	7.44e-3	-1.52e-3
060609	-7.88e-3	9.79e-3	-1.27e-3

Table 2 Coarse estimation of 3D gyro biases

Test	Gyro biases in BF (rad)		
	x	y	Z
060531	9.79e-6	1.35e-5	-1.2e-5
060601	6.37e-6	7.86e-6	-1.7e-5
060607	8.61e-6	9.70e-6	-1.5e-5
060608	6.47e-6	7.14e-6	-1.5e-5
060609	6.44e-6	7.06e-6	-1.3e-5

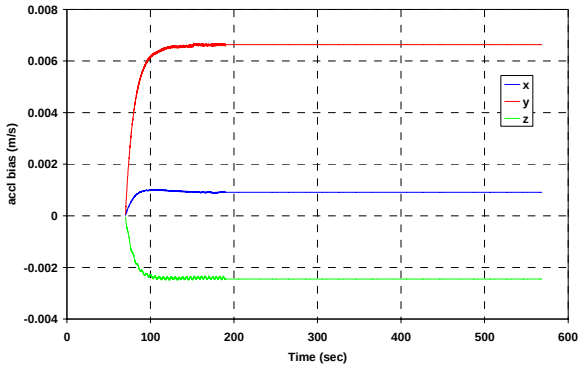

Fig. 4 Tri-axial accelerometer bias estimates versus time

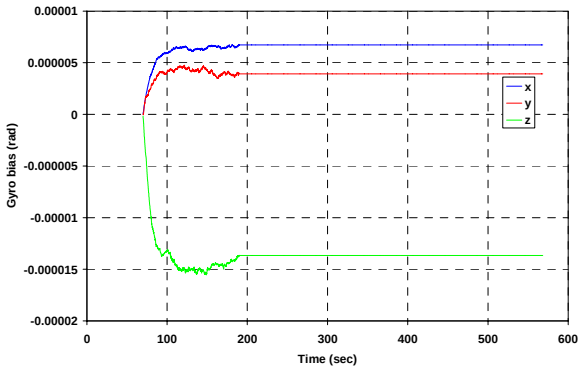

Fig. 5 Tri-axial gyro bias estimates versus time

The coarse estimates of the sensor biases were then used in the integration Kalman filter for the fine alignment step. Because the system was static during the alignment process, the zero velocity and averaged GPS position were used in the fine

alignment process. Although the visible GPS satellite constellation and the satellites' position and velocity errors still impact on the sensor bias estimates, the GPS measurement errors were isolated from the sensor bias estimates. This approach provides a window to observe how the filter accurately tracks the sensor errors without the influence of the GPS measurement errors.

Different EKF and the SPKF-derived solutions were obtained using the same values of the filter parameters, i.e., the initial state vector, the initial state covariance, the system noise covariance, and the measurement noise covariance. To obtain similar solutions from the EKF and SPKF, some parameters must be set to different values for the two filters. For example, the square-root of covariance of the accelerometer noise must be set to 0.0021g for the EKF and 0.0022g for the SPKF, with the rest of the parameters having the same values for the two filters.

With the parameter settings above, the two filtering results that were obtained are very close. The SPKF estimates of the sensor biases and the covariance of the estimation errors are shown in Figs. 6-11. It can be seen that the filter converges after about 700 seconds. This is obtained from the filtering with a 1Hz update rate. A faster convergence could be achieved using a higher filter update rate, for example if the filter updates at every SDINS output, in which case the filter can converge within 2 minutes.

Because the feedback correction is applied, the sensor bias estimates become smaller and smaller during the filtering operation, as shown in Figs. 6-9. The vertical accelerometer bias estimate depicted in Fig. 7 looks different from the horizontal components depicted in Fig. 6. As can be seen in Eq. (39), the coarse estimate of the vertical accelerometer bias is insensitive to the misalignment angles, thus the coarse estimate of the vertical accelerometer bias is so accurate that the improvement from the filter is limited. This is also reflected in the covariance-time curve in Fig. 10, where it is easy to see that the z-component converges faster than the other two components.

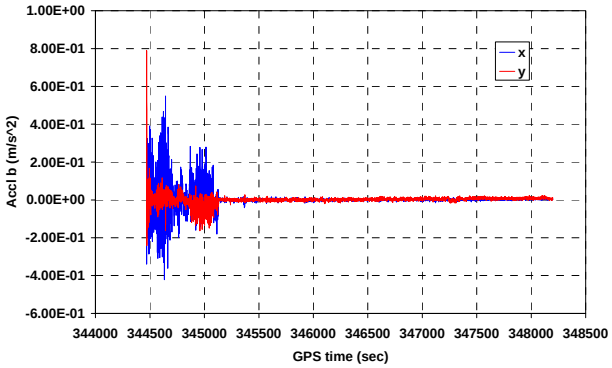

Fig. 6 Horizontal accelerometer bias estimates

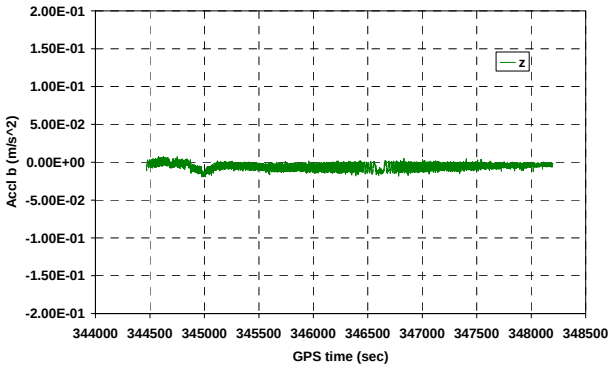

Fig. 7 Vertical accelerometer bias estimate

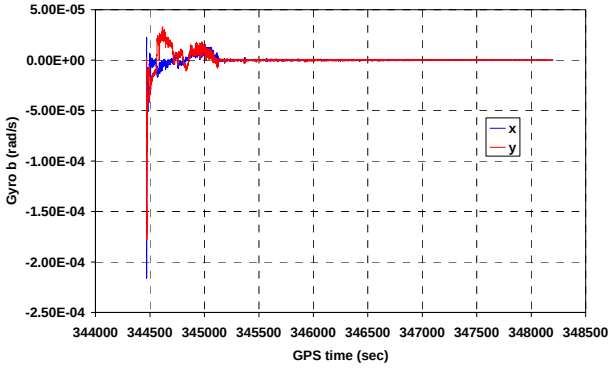

Fig. 8 Horizontal gyro bias estimates

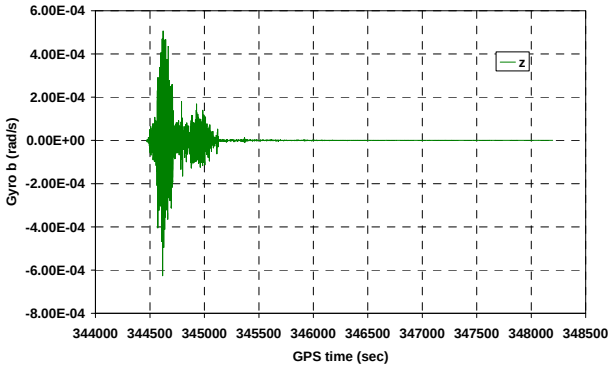

Fig. 9 Vertical gyro bias estimate

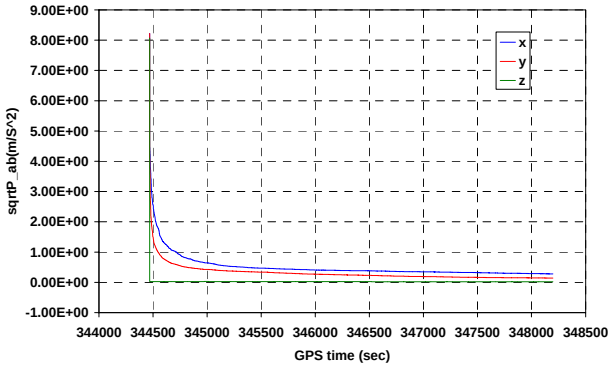

Fig. 10 Square root of the covariance of the accelerometer bias estimates

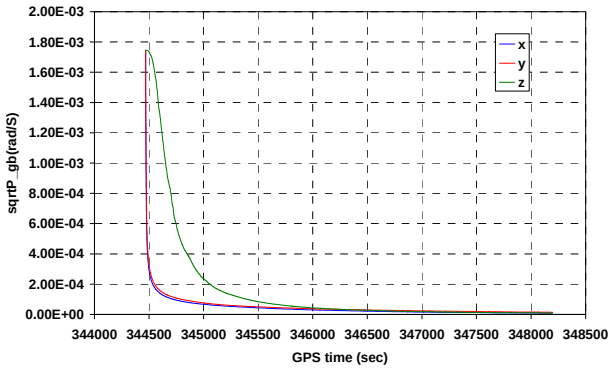

Fig. 11 Square-root of the covariance of the gyro bias estimates

The SDINS solution converges to a stable value when the sensor biases estimates are stable. Because the sensor biases directly affect the velocity and attitude solution, the corrected velocity and attitude solutions can be used to evaluate the sensor bias estimates. Figs. 12 and 13 show the velocity and attitude solutions from the EKF. Figs. 14 and 15 are the velocity and attitude solutions from the SPKF. The corrected solutions from the SPKF and the EKF are very close when the solution becomes stable. However, the transient periods for the two filters are quite different. Comparing Figs. 12 and 14, it can be seen that the SPKF has smaller errors during the transient period. A similar conclusion is drawn for the attitude solution except for the azimuth (z-component), see Figs. 13 and 14.

As can be seen in Figs. 13 and 15, the azimuth angle (z-component) from either the EKF or the SPKF converges slower than the other two components. It appears to wander.

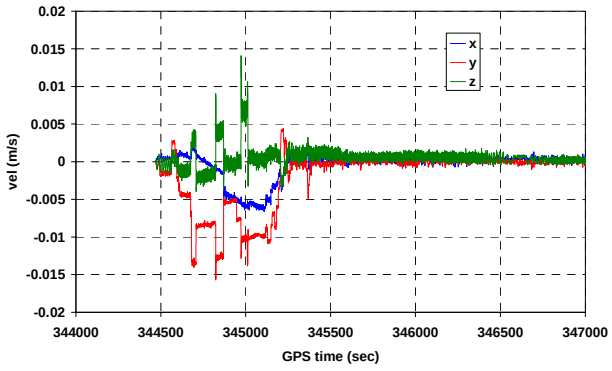

Fig. 12 SDINS velocity solution with sensor biases compensation from the EKF

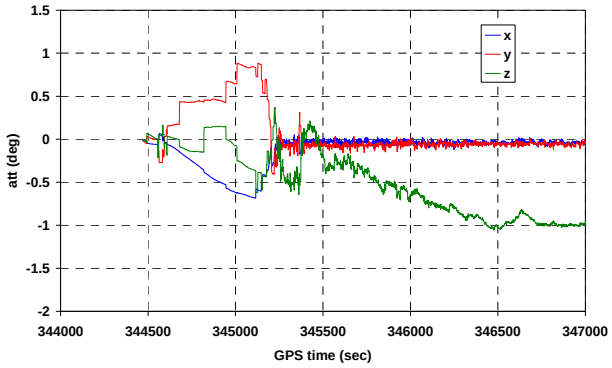

Fig. 13 SDINS attitude solution with sensor biases compensation from the EKF

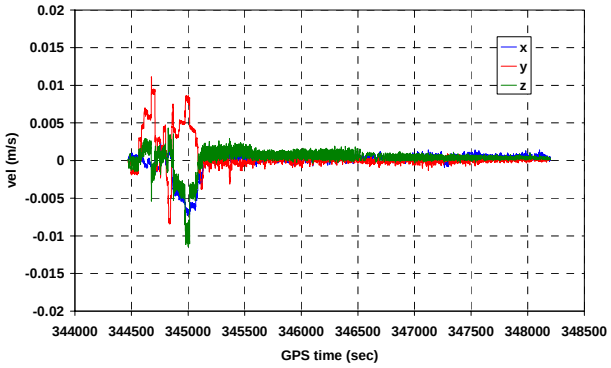

Fig. 14 SDINS velocity solution with sensor biases compensation from the SPKF

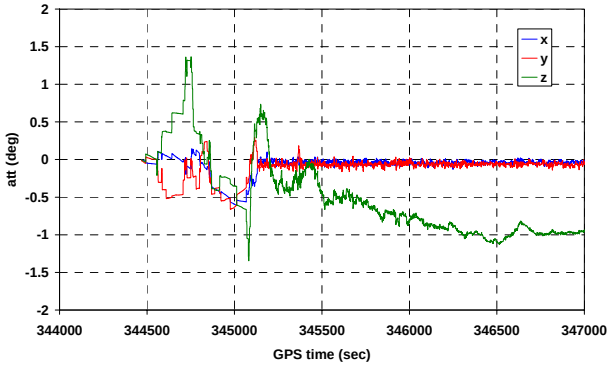

Fig. 15 SDINS attitude solution with sensor biases compensation from the SPKF

6. CONCLUSIONS

A procedure based on nonlinear filtering methods has been implemented for inertial sensor bias estimation through the integration of GPS and INS. The procedure can be implemented in three sequential steps: the coarse alignment, the fine alignment, and the integration filtering. An algorithm has been presented for the coarse estimation of the inertial sensor biases from the accelerometer and gyro measurements. The coarse estimates of the sensor biases are subsequently used in the fine alignment - for the refined estimates of the sensor biases. Two nonlinear filters, the EKF and the SPKF, are used in the fine alignment.

The two filters' performances are very similar in terms of tracking the sensor biases, and in terms of the convergence speed. The two filtering solutions are very close after the filters converge, however they perform quite differently during the transient period. From a comparison of the sensor-calibrated SDIN solutions it is found that the SPKF has smaller errors in the tilt angles and velocity during the transient period. The azimuth angle has a slower convergence speed in comparison to the tilt angles for both the SPKF and the EKF.

ACKNOWLEDGMENTS

The project is funded under the Australian Cooperative Research Centre for Spatial Information (CRC-SI). The authors would like to acknowledge the support from the CRC-SI.

REFERENCES

1. D. A. Grejner-Brzezinska, R. Da, and C. Toth, *GPS Error Modelling and OTF Ambiguity Resolution for High-Accuracy GPS/INS Integrated System*, Journal of Geodesy, Vol.72, 1998, pp. 626-638.
2. M. K. Martin and B. C. Detterich, C-MIGITS II Design and Performance, Proceedings of ION GPS-97, Kansas City, Kansas, September 16-19, 1997, pp. 95-102.

3. R. Da, *Investigation of a Low-Cost and High-Accuracy GPS/IMU System*, Proceedings of ION National Technical Meeting 1997, Santa Monica, California, January 14-16, 1997, pp. 955-963.
4. R. Van der Merwe, and E. A. Wan, *Sigma-point Kalman Filters for Integrated Navigation*, Proceedings of the 60th Annual Meeting of The Institute of Navigation, Dayton, Ohio, June 7-9, 2004, pp. 641-654.
5. J. Wendel, J. Metzger, R. Moenikes, A. Maier, G. F. Trommer, *A Performance Comparison of Tightly Coupled GPS/INS Navigation Systems Based on Extended and Sigma Point Kalman Filters*, Proceedings of ION GNSS 2005, Long Beach, California, September 13-16 , 2005, pp. 456-466.
6. C. K. Cui and G. Chen, *Kalman Filtering*, 3rd Ed, Springer, 1999.
7. S. J. Julier and J. K. Uhlmann, *Unscented Filtering and Nonlinear Estimation*, Proceedings of the IEEE, Vol. 92, No. 3, 2004, pp. 401-422.
8. S. Julier, J. Uhlmann, and H. F. Durrant-Whyte, *A New Method for the Nonlinear Transformation of Means and Covariances in Filters and Estimators*, IEEE Trans On AC, Vol. 45, No. 3, 2000, pp. 477-482.
9. T. Lefebvre, H. Bruyninckx, and J. De Schutter, *Comment on "A New Method for the Nonlinear Transformation of Means and Covariances in Filters and Estimators"*, IEEE Trans on AC, Vol. 47, No. 8, 2002, pp. 1406-1408.
10. Y. Li, J. Wang, C. Rizos, P. Mumford, and W. Ding, *Low-cost Tightly Coupled GPS/INS Integration Based on a Nonlinear Kalman Filtering Design*, Proceedings of ION National Technical Meeting 2006, Monterey, California, January 18-20, 2006, pp. 958-966.
11. S. J. Julier and J. K. Uhlmann, *Reduced Sigma Point Filters for the Propagation of Means and Covariances through Nonlinear Transformations*, http://www.cs.unc.edu/~welch/kalman/media/pdf/ACC02-IEEE1358.pdf, accessed on September 1, 2005.
12. G.R. Pitman, Jr., Ed., *Inertial Guidance*, John Wiley and Sons, New York, 1962.
13. Y. Li, A. Dempster, B. Li, J. Wang, and C. Rizos, *A Low-cost Attitude Heading Reference System by Combination of GPS and Magnetometers and MEMS Inertial Sensors for Mobile Applications*, The International Symposium on GPS/GNSS 8-10 December 2005, Hong Kong. paper 5A-01, CD-ROM procs.
14. I. Y. Bar-Itzhack, *Navigation Computation in Terrestrial Strapdown Inertial Navigation System*, IEEE Trans. On AES, Vol. AES-13, No. 6, 1977, pp. 679-689.
15. I. Y. Bar-Itzhack and N. Berman, *Control Theoretical Approach to Inertial Navigation Systems*, Journal of Guidance, Control and Dynamics, Vol. 11, No. 3, 1988, pp. 237-245.
16. P. J. David, E.N. Abbas, ed., *Feedback Control System*, Prentice Hall: New Jersey, 4th ed., 2002.
17. Y. Li, P. Mumford, J. Wang, and C. Rizos, *Development of a GPS/INS Integrated System on the Field Programmable Gate Array Platform*, Proceedings of ION GNSS 2006, Forth Worth, Texas, September 26-30, 2006.